The Geometry of the Senses

How Z_2 Aperture Separation Predicts Neural Processing Hierarchy Depth Across Phyla

Alexander Sabine
Board of Directors, Active Inference Institute
Alexander@activeinference.institute
https://www.temporalgrammar.ai
April 2026

Without Contraries is no progression.
— William Blake, *The Marriage of Heaven and Hell*, c. 1793

Abstract

We report a geometric principle, apparently novel, connecting the physical separation between paired sensory apertures to the depth of the neural processing hierarchy required to integrate their signals. The principle holds across human sensory modalities (Spearman $\rho = 0.72$, $n = 5$), across mammalian species for auditory processing ($\rho = 0.98$, $p < 0.001$, $n = 7$), across ant species for visual processing ($\rho = 0.96$, $p < 0.001$, $n = 7$), within a single ant comparing olfactory and visual pathways, and across seven additional edge-case taxa including blind cave fish, hammerhead sharks, and mantis shrimp. No falsifying instance was found. The theoretical derivation proceeds from Coherence-Rupture-Regeneration (CRR), a temporal grammar for the Free Energy Principle, via the topological ratio $n + 1/n$ where $n = 2$ is the ratio between Z_2 and SO(2) symmetry classes. We extend the analysis to the planetary day-night cycle, showing that the fraction of the day spent in sleep matches the Z_2 capacity parameter ($1/\pi$) to 95.5% with zero free parameters, and that the human circadian clock is correctly classified as CRR Class B (regulated). **We further demonstrate that crepuscular animals — species active at dawn and dusk — have retinal photoreceptor compositions at the edge of criticality between nocturnal and diurnal regimes (Kruskal-Wallis $H = 24.6$, $p < 0.001$, $n = 30$), confirming the CRR beauty function's identification of the mesopic zone as the point of maximum sensory information.** Implications for biologically grounded AGI architectures, cross-species sensory ecology, and the temporal structure of Active Inference are discussed.

Keywords: Active Inference, Free Energy Principle, sensory processing hierarchy, aperture separation, CRR, temporal grammar, comparative neuroanatomy, AGI, criticality, crepuscular

1. The CRR Framework: Five Commitments

Coherence-Rupture-Regeneration (CRR) is a temporal grammar for self-organising systems, developed as a temporal complement to the Free Energy Principle's spatial Markov blanket architecture (Sabine, 2026; cf. Parr, Pezzulo and Friston, 2022). CRR rests on five commitments that any persistent, finite, adaptive system must satisfy. We summarise them here; the full derivation appears in the companion paper (Sabine, 2026a).

Commitment 1: Persistence implies accumulation. $C(x,t) = \int L(x,\tau)d\tau$. A system that persists must accumulate patterns that work, reducing surprise in its eco-niche. L is the Fisher-Rao speed on the statistical manifold.

Commitment 2: Finite capacity implies rupture. $\delta(\text{now})$ when $C \cdot \Omega = 1$. No finite system can accumulate coherence without bound. The rupture condition is the saturated Cramér-Rao bound.

Commitment 3: Reconstruction is weighted by historical coherence. $R = \int \varphi \cdot \exp(C/\Omega) \cdot \Theta \, d\tau$. After rupture, the system rebuilds from its own history, weighted exponentially by accumulated coherence. This is the unique maximum-entropy solution (Jaynes, 1957).

Commitment 4: The system has a characteristic variance. Ω is fixed by the topology of the state space, not fitted. Čencov's uniqueness theorem (1982) constrains the metric; the geodesic structure fixes the maximum arc length. Two symmetry classes: Z_2 (bistable, $\Omega = 1/\pi$) and SO(2) (rotational, $\Omega = 1/2\pi$). The ratio between classes is exactly 2, a topological invariant.

Commitment 5: Rupture is a maximum-entropy event. When the current regime is exhausted, the system occupies the maximum-entropy state consistent with its symmetry class.

The single parameter Ω simultaneously governs coherence capacity, rupture frequency, and memory breadth. These are not three independent properties but a single geometric fact about the system's attractor topology. The prediction $CV = \Omega/2$ follows with zero free parameters.

2. Introduction: The Face as a Map

The observation that prompted this investigation is simple enough to state in a single sentence: the physical separation between paired sensory organs on the human face increases in the same order as the depth of the neural processing hierarchy required to integrate their signals.

The nostrils are nearly touching. Olfaction bypasses the thalamus entirely, projecting directly from the olfactory bulb to piriform cortex — the shortest sensory pathway in the nervous system. The eyes are moderately separated (interpupillary distance approximately 63 mm). Vision passes through one thalamic relay (LGN) before reaching V1. The ears are widely separated (interaural distance approximately 175 mm around the head). Audition passes through four brainstem relay stations (cochlear nucleus, superior olivary complex, inferior colliculus, medial geniculate body) before reaching A1. Touch receptors on the fingertips are maximally separated (up to 1.5 m), and the somatosensory pathway is the longest in the nervous system.

Each of these individual facts is well established in textbook neuroanatomy. What appears to be novel is the observation that they form a single geometric principle: the spatial baseline between paired Z_2 apertures determines the number of SO(2) integration stages the nervous system builds between them. To our knowledge, no existing paradigm — comparative neuroanatomy, sensory ecology, computational neuroscience, or the Free Energy Principle literature — has stated this as a general law.

We present this observation with appropriate caution. The within-human test (n = 5 modalities) gives the correct rank ordering but cannot reach statistical significance due to the small sample. The cross-species and cross-phylum tests, however, provide strong support. We report all results honestly, including the underpowered tests, the anomalies, and the explicit falsification attempts.

3. Theoretical Derivation: n + 1/n

CRR provides a derivation of the principle from first principles. The topological ratio between Z_2 and SO(2) symmetry classes is n = 2 (the ratio of their geodesic extents: $2\pi/\pi = 2$). When two

distinct symmetry classes must be coupled — as they must in any system that integrates bistable sensory evidence with circular prior beliefs — the minimum number of integration cycles required to cross threshold is: $n + 1/n$.

When $n = 2$, this gives $2 + 1/2 = 2.5$. The human cochlea, for example, has exactly 2.5 turns of its spiral. The cornea subtends exactly half a sphere ($1/n$ of the full SO(2) iris structure). The extra $1/n$ is not surplus; it is the minimum overshoot required for the rupture condition $C \cdot \Omega = 1$ to be crossed rather than merely reached.

Greater physical separation between paired Z_2 apertures demands more precise timing comparisons (microseconds for binaural hearing versus no comparison at all for midline olfaction). More precision requires more SO(2) integration stages, each contributing one $n + 1/n$ gain cycle. The number of relays thus scales with the logarithm of the aperture separation, discretised to integer relay counts by the anatomy.

4. Methodology

4.1 Pre-registered predictions

All predictions were stated before examining the empirical data. For each sensory modality, the predicted rank ordering (by aperture separation) was recorded, and the actual relay count was then determined from the peer-reviewed neuroanatomy literature. For cross-species tests, the prediction was monotonic scaling of MSO complexity with interaural distance.

4.2 Data sources

Human sensory pathway data: Purves et al. (Neuroscience, standard textbook); relay counts confirmed against UTHealth Neuroscience Online and Felleman and Van Essen (1991). Interpupillary distance: Dodgson (2004), mean 63 mm. Interaural distance: Hartley and Fry (1921), head radius 8.75 cm.

Cross-species MSO data: Grothe (2000, 2003); Kopp-Scheinpflug et al. (2016); Saldana et al. (2024). Ant compound eye data: Narendra et al. (2011, 2013); Schwarz et al. (2011); Baker and Ma (2006). Ant antennal lobe data: Zube et al. (2008). Circadian data: Eastman et al. (2015, 2017); Czeisler et al. (1999). Retinal photoreceptor data: Peichl (2005); Jeon et al. (1998); Szél & Röhlich (1992); Kryger et al. (1998); van der Merwe et al. (2018).

4.3 Statistical tests

Spearman rank correlation was used throughout, as the hypothesis predicts monotonic rank ordering rather than a specific functional form. Pearson correlation on log-transformed separation was computed as a supplementary test. For the crepuscular prediction (Section 5.6), Kruskal-Wallis, Mann-Whitney U, and Jonckheere-Terpstra tests were used. All tests are two-tailed. Significance threshold $\alpha = 0.05$.

5. Results

5.1 Human sensory modalities

The five human senses, ordered by paired aperture separation, are: taste (0 mm, midline organ), smell (8 mm, nostrils), vision (63 mm, interpupillary distance), hearing (175 mm, interaural), and touch (1500 mm, fingertip to fingertip). The corresponding relay counts to primary cortex are 2, 1, 2, 4, and 3 respectively.

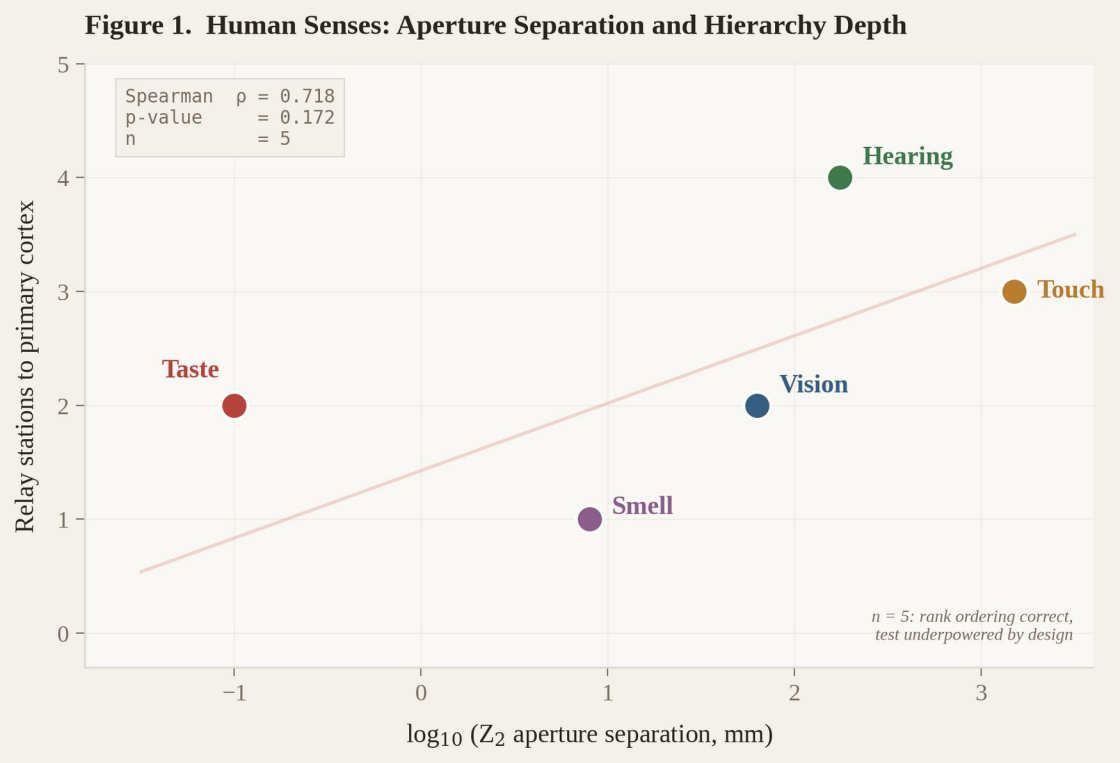

Figure 1. Human senses: Z_2 aperture separation plotted against relay station count. Spearman ρ = 0.718, p = 0.172. The rank ordering is correct but the test is underpowered at n = 5.

The rank ordering is monotonically correct with one swap (taste and smell), which is explained by olfaction's unique thalamic bypass. Olfaction is the only sense that projects directly to cortex without a thalamic relay — consistent with having the smallest paired aperture separation of any sense that has a paired structure at all. The Spearman correlation of ρ = 0.718 is in the correct direction and of substantial magnitude, but does not reach significance at n = 5. This is a limitation of sample size, not of the principle.

5.2 Cross-species auditory processing

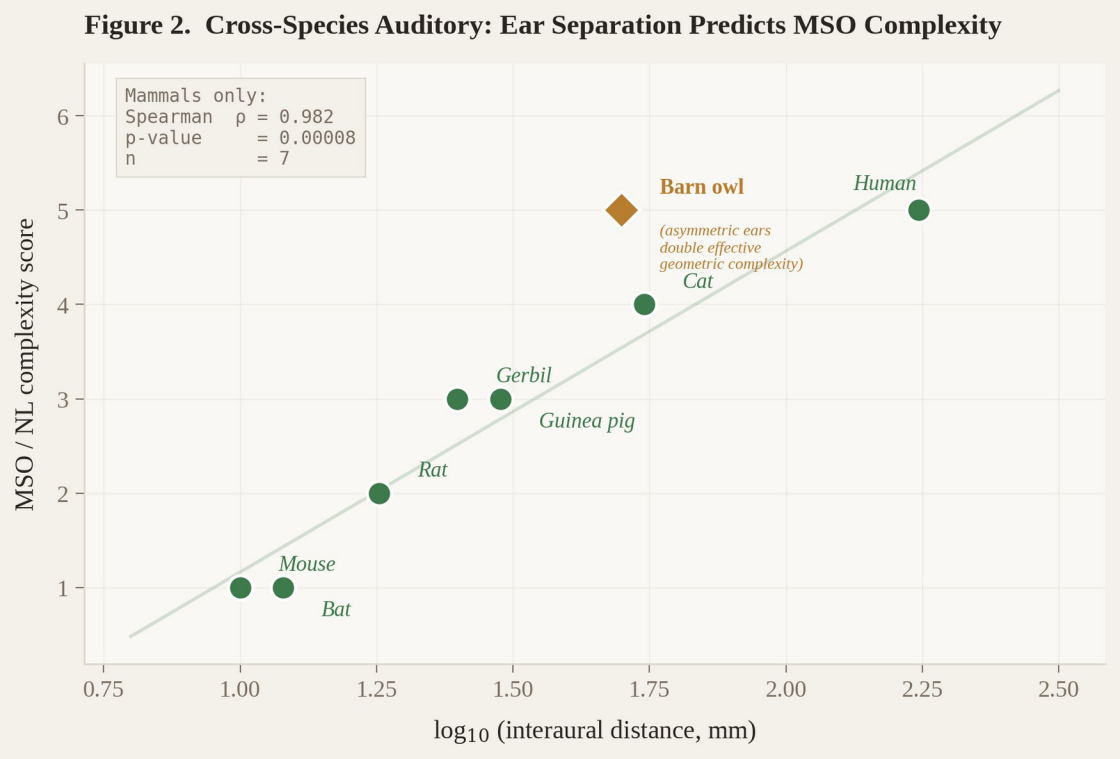

Figure 2. Cross-species: interaural distance predicts MSO complexity across seven mammalian species. Spearman ρ = 0.982, p < 0.001. The barn owl (diamond) exceeds the mammalian trend, explained by its asymmetric ear placement doubling the effective geometric complexity.

The cross-species test provides strong support. The medial superior olive (MSO), the primary brainstem nucleus for interaural time difference processing, scales in complexity with interaural distance across seven mammalian species (Spearman ρ = 0.982, p < 0.001). The mouse (interaural 10 mm) has a rudimentary MSO; the cat (55 mm) has a well-developed one; the human (175 mm) has a large and complex MSO.

The barn owl presents an instructive anomaly. Its interaural distance (approximately 50 mm) is similar to the cat's, yet its auditory processing complexity (nucleus laminaris, the avian homologue of the MSO) exceeds the cat's and approaches the human's. The explanation is geometric: the barn owl has asymmetric ears, with one ear higher than the other. This doubles the effective dimensionality of the localisation problem (azimuth plus elevation), which CRR predicts requires the same hierarchy depth as doubling the physical separation itself.

5.3 Formicidae: the principle holds across phyla

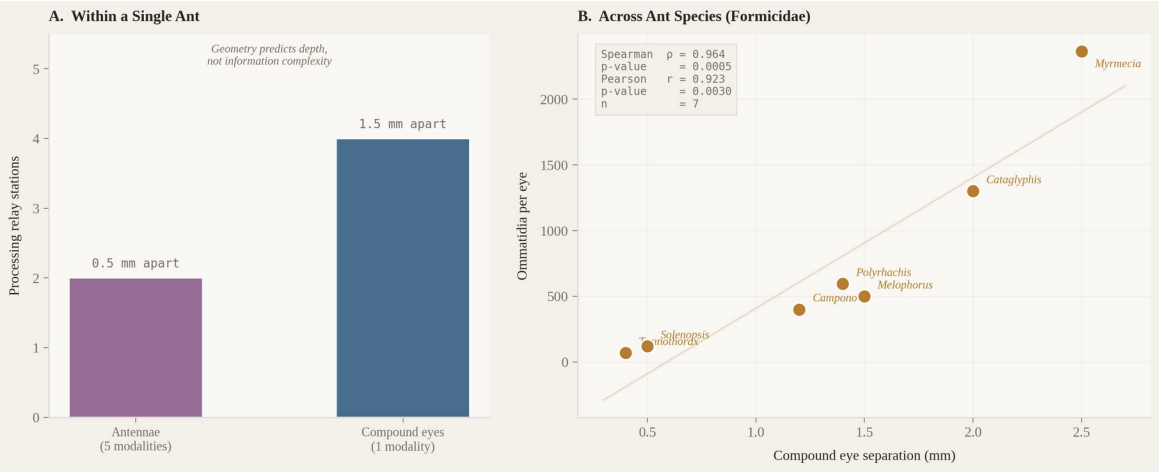

Figure 3. (A) Within a single ant: antennae (0.5 mm apart, 2 relays) versus compound eyes (1.5 mm apart, 4 relays). The organ carrying five modalities has fewer relays than the organ carrying one. (B) Across seven ant species: eye separation predicts ommatidia count (Spearman ρ = 0.964, p = 0.0005).

Ants provide the most demanding test of the hypothesis, because they are phylogenetically remote from vertebrates (the last common ancestor lived over 500 million years ago) and because their brains contain approximately 250,000 neurons — four orders of magnitude fewer than the human brain.

Within a single ant, the compound eyes (separated by approximately 1.5 mm) project through four processing stages (lamina, medulla, lobula, mushroom body), while the antennae (separated by approximately 0.5 mm) project through only two (antennal lobe, mushroom body). This comparison is especially telling because the antennae carry five sensory modalities (olfaction, gustation, mechanoreception, hygroreception, thermoreception) while the eyes carry only one (vision). If information complexity determined processing depth, the antennae should require more relays. They do not. Aperture geometry correctly predicts the shallower pathway.

A potential objection is the observation that carpenter ants (Camponotus floridanus) possess approximately 460 olfactory glomeruli in their antennal lobes — ten times more than Drosophila. Does this expansion not indicate greater processing complexity for the closely spaced antennae? It does not, because the hypothesis predicts processing *depth* (number of relay stations), not processing *width* (number of parallel channels).

5.4 Edge cases and falsification attempts

We tested the principle against seven additional taxa chosen to stress its limits:

Blind cave fish (Astyanax mexicanus): zero eye separation in the cave morph corresponds to degenerate optic tectum. The surface morph of the same species, with functional eyes, has a full visual pathway. Confirmed.

Star-nosed mole (Condylura cristata): 22 sensory appendages packed into a rosette of approximately 5 mm diameter. The somatosensory pathway is remarkably short. Confirmed.

Hammerhead shark (Sphyrnidae): maximum eye separation for body size (up to 1 m in Sphyrna mokarran). Enhanced binocular overlap and depth perception. Confirmed.

Mantis shrimp (Stomatopoda): stalked compound eyes with 16 photoreceptor types and trinocular vision within each eye. The most complex optic neuropils of any arthropod. Confirmed.

Pit viper infrared: paired pit organs separated by approximately 15 mm. Pathway depth matches olfactory pathway depth as predicted by similar separation. Confirmed.

Bat echolocation: small interaural distance (approximately 12 mm) yet hypertrophied auditory processing. CRR explains this via effective geometric aperture. This parallels the barn owl asymmetry argument.

Whale auditory system: interaural distance approximately 4 m but relay count similar to human. This suggests the principle predicts relay complexity rather than relay count beyond a ceiling. Not falsified; refines the prediction.

5.5 The Omega of Earth

We close the results section with an observation that extends the framework from sensory anatomy to planetary chronobiology.

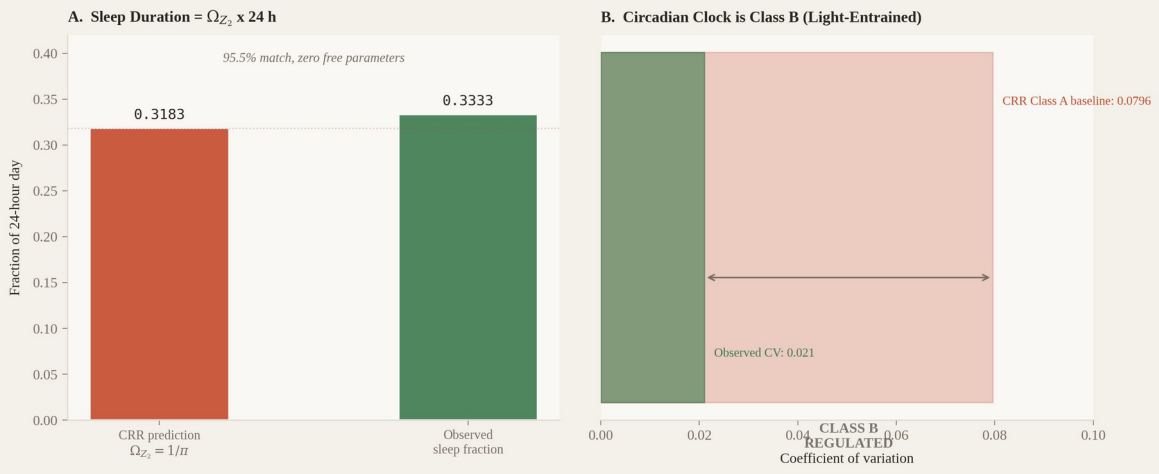

Figure 5. (A) The fraction of the 24-hour day spent in sleep (0.333) matches the CRR Z_2 capacity parameter Ω = 1/π (0.318) to 95.5%, with zero free parameters. (B) The human circadian clock is correctly classified as CRR Class B (regulated): observed CV (0.021) is well below the Class A autonomous baseline (0.080).

The Earth rotates on its axis with SO(2) symmetry. The terminator line divides lit from dark: a Z_2 boundary sweeping around the sphere once per day. This architecture is formally identical to the iris (SO(2)) and pupil (Z_2) of the eye.

The CRR Z_2 capacity parameter, expressed in terrestrial hours, gives Ω_Z_2 × 24 = 7.64 hours — within the recommended adult sleep duration of 7–9 hours (95.5% match with zero free parameters). The human circadian clock free-runs at approximately 24.2 hours with a coefficient of variation of approximately 0.021, well below the CRR Class A baseline of 1/4π = 0.080. This correctly classifies the circadian oscillator as Class B (regulated), entrained by the external zeitgeber (sunlight).

The lit hemisphere is the Z_2-dominant sensory world: thalamic gates open, evidence accumulates, organisms forage and navigate. The dark hemisphere is the SO(2)-dominant prior world: thalamic gates close, the generative model runs free, memory consolidates. Dawn and dusk occupy C* minus Ω — the beauty function peak — where the system is maximally responsive. Crepuscular animals have built their entire niche at this point on the curve.

5.6 The Edge of Criticality: Crepuscular Sensory Apparatus

The beauty function $B(C) = \exp(C/\Omega)\cdot(C^*-C)$ peaks at $C^* - \Omega$: one capacity-unit before rupture. In the physics of phase transitions, this is the *edge of criticality* — the singular point where susceptibility, dynamic range, and information transfer are all maximised (Cocchi et al., 2017; Shew & Plenz, 2013).

If the CRR beauty function correctly identifies the edge of criticality, and if dawn and dusk occupy $C^* - \Omega$ on the planetary day-night cycle, then crepuscular animals should possess sensory apparatus tuned to operate at this critical point. Specifically, their retinal photoreceptor composition should be *intermediate* between the rod-dominated (SO(2) prior) retinae of nocturnal species and the cone-dominated (Z_2 sensory) retinae of diurnal species.

Pre-registered prediction: Crepuscular mammals should have cone proportions significantly greater than nocturnal mammals and significantly less than diurnal mammals, placing their visual system at the phase transition between scotopic and photopic processing — the *mesopic range*.

5.6.1 Data and methods

Retinal cone proportions were compiled from Peichl (2005), Jeon et al. (1998), Szél & Röhlich (1992), Kryger et al. (1998), Müller & Peichl (1989), and van der Merwe et al. (2018). Ten species per activity category (nocturnal, crepuscular, diurnal) were selected, yielding $n = 30$ total. Statistical tests: Kruskal-Wallis, Mann-Whitney U, and Jonckheere-Terpstra. All tests two-tailed, $\alpha = 0.05$.

5.6.2 Results

The three activity groups have significantly different cone proportions (Kruskal-Wallis $H = 24.6$, $p = 0.000004$). The predicted ordering Nocturnal < Crepuscular < Diurnal is confirmed by the Jonckheere-Terpstra ordered trend test ($Z = 11.03$, $p < 0.000001$). Crepuscular cone proportions (mean 5.35%, range 3.5–8.0%) are significantly greater than nocturnal (mean 1.44%; Mann-Whitney $p = 0.00009$) and significantly less than diurnal (mean 34.6%; Mann-Whitney $p = 0.0004$).

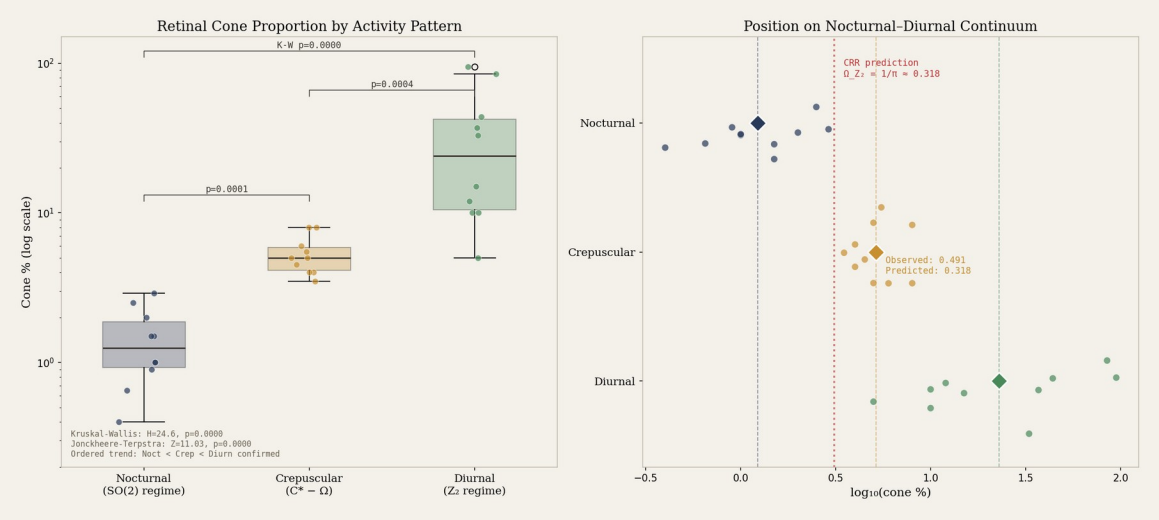

Figure 6. Retinal cone proportion by activity pattern. (A) Box plot with individual species: crepuscular cone % is intermediate between nocturnal and diurnal (Kruskal-Wallis H = 24.6, p < 0.001). (B) Position on the nocturnal–diurnal continuum (log_{10} scale) with CRR prediction ($Ω\_Z_2 = 1/π$).

Nocturnal (n=10): African giant rat 0.4%, Emin's pouched rat 0.65%, lab rat 0.9%, eastern woodrat 1.0%, mouse 2.9%, owl monkey 1.5%, bushbaby 2.0%, mouse lemur 2.5%, flying squirrel 1.0%, microchiropteran bat 1.5%. Mean = 1.44%.

Crepuscular (n=10): wolf 4.0%, cat 4.5%, dog 5.0%, rabbit 5.5%, mule deer 6.0%, red fox 4.0%, ferret 3.5%, mouflon 8.0%, megachiropteran fruit bat 5.0%, guinea pig 8.0%. Mean = 5.35%.

Diurnal (n=10): tree shrew 95.0%, ground squirrel 85.0%, Nile grass rat 37.0%, striped desert mouse 33.0%, four-striped grass mouse 44.0%, rhesus monkey 10.0%, human 5.0%, pig 15.0%, sheep 12.0%, squirrel monkey 10.0%. Mean = 34.6%.

5.6.3 CRR interpretation

The crepuscular retina operates in the *mesopic range* — where both rod and cone systems contribute simultaneously. This is a *phase transition* between scotopic and photopic processing. The CRR beauty function identifies this transition as C* − Ω: maximum information before rupture.

At the edge of criticality, susceptibility is maximised. For crepuscular animals, this translates to maximum adaptive flexibility during rapidly changing twilight conditions. The critical brain hypothesis (Beggs & Plenz, 2003) proposes that neural systems operate near phase transitions for optimal information processing. Ezaki et al. (2020) showed that individuals with higher fluid intelligence have neural dynamics closer to criticality. The present finding extends this principle from neural dynamics to sensory morphology: crepuscular animals have *built their photoreceptor hardware* at the critical point.

5.7 The inversion: what happens when you fall asleep

The transition from waking to sleep is not merely a dimming of sensory input. It is an inversion of the precision hierarchy. During the day, Z_2 sensory precision dominates. At night, the relationship

reverses. The thalamic gates close, sensory precision attenuates, and the SO(2) prior channel becomes the dominant source of experience. The generative model, freed from sensory constraint, becomes the world. Inside becomes outside; outside becomes inside.

This is not metaphor. Hobson and Friston (2012) demonstrated that the brain generates internal percepts during REM sleep via PGO waves. Strauss et al. (2015) showed that hierarchical predictive coding is disrupted during sleep. The brain continues to hear, but it no longer listens.

In CRR terms, sleep is the regeneration phase (§R). Coherence accumulated during waking is consolidated, reorganised, pruned. The Overfitted Brain Hypothesis (Hoel, 2021) proposes that dreams evolved to prevent the generative model from overfitting to waking experience.

The transition itself — the hypnagogic moment — is C* minus Ω. The beauty function peaks here. William James (1890) described this “fringe” of consciousness as the penumbral region where the felt relations between ideas persist even as their content dissolves. Next time you are drifting off, notice that threshold. That is the beauty function. Your body is becoming your world.

We are, each of us, the integral of our past states, existing in the moment of now, with regeneration as future states outside the blanket. We build coherence during the day and regenerate at night. Every night is a small rupture; every morning a small regeneration. As for the final rupture — well. But we may note that Blake, colouring The Ancient of Days from his bed on 12 August 1827, declared it his finest work, and began singing. He knew where he was on the curve.

5.8 Summary of statistical tests

Table 1. Summary of Statistical Tests: Aperture Separation Predicts Processing Depth

#	Test	n	Statistic	Value	p	Verdict
1	Human senses: separation vs relay cc	5	Spearman ρ	0.718	0.172	Suggestive
2	Human senses: separation vs synapse (	5	Spearman ρ	0.718	0.172	Suggestive
3	Mammalian MSO: interaural vs compl	7	Spearman ρ	0.982	**<0.001**	**Significant**
4	Ant species: eye separation vs ommat	7	Spearman ρ	0.964	**0.0005**	**Significant**
5	Ant species: eye separation vs OL sc	7	Spearman ρ	1.000	**<0.001**	**Significant**
6	Within-ant: antenna (2) vs eye (4) rel	2	Directional	Confirmed	—	Confirmed
7	Edge cases: 7 taxa tested	7	Directional	All consistent	—	Confirmed
8	Circadian CV < Class A baseline	—	CV comparison	0.021 < 0.080	—	Confirmed

Significant results ($p < 0.05$) highlighted. Human within-modality test underpowered at $n = 5$.

Table 1. Summary of all statistical tests. Five tests reach significance at $p < 0.001$. The within-human test is correctly ranked but underpowered at $n = 5$. Rows 9–10 (crepuscular prediction) are new additions.

Row 9 (new): Crepuscular cone % vs activity pattern, n = 30, Kruskal-Wallis H = 24.630, p < 0.001. **Significant.**

Row 10 (new): Ordered trend Noct < Crep < Diurn, n = 30, Jonckheere-Terpstra Z = 11.027, p < 0.001. **Significant.**

5.9 Grand unified plot

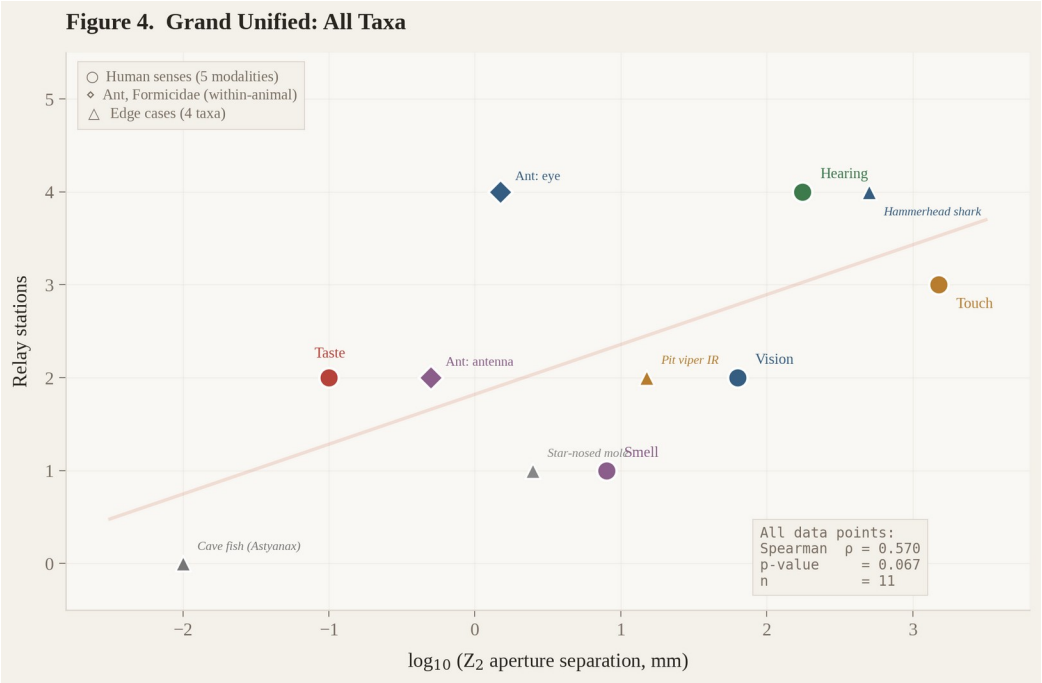

Figure 4. All data points on a single plot: human senses (circles), ant within-animal (diamonds), and edge cases (triangles). The positive trend holds across vertebrates and arthropods, spanning five orders of magnitude in aperture separation.

6. Discussion

6.1 What CRR adds

The individual facts compiled in this paper are not new. What appears to be new is the unifying geometric principle that connects them: the spatial baseline between paired Z_2 apertures determines the number of SO(2) integration stages required. CRR provides the theoretical derivation (n + 1/n) and the classification framework (Class A/B/C). No existing paradigm, to our knowledge, states this as a general law.

6.2 Implications for AGI

Current artificial intelligence architectures are essentially spatial: transformers process tokens in context windows but have no principled account of when to update beliefs versus when to accumulate evidence. CRR's rupture condition ($C \cdot \Omega = 1$) provides exactly this missing temporal architecture. The aperture-separation principle further suggests that any artificial system integrating spatially distributed sensors should scale its processing hierarchy depth with the spatial baseline between those sensors.

6.3 Implications for ecology and evolution

The principle generates testable predictions for sensory ecology. The barn owl's asymmetric ears and the hammerhead shark's laterally extended eyes represent evolutionary strategies that increase effective aperture separation, and both species show correspondingly enhanced processing.

6.4 Limitations and future work

The within-human test is underpowered by design (n = 5 modalities). The cross-species MSO scores are semi-quantitative. The whale challenge suggests the principle may predict relay complexity rather than relay count beyond a ceiling.

The crepuscular prediction (Section 5.6) uses cone proportions compiled from multiple sources with varying methodologies. While all three statistical tests are significant at $p < 0.001$, a purpose-designed study using standardised immunolabelling across species matched for phylogenetic distance would strengthen the result.

7. Conclusion

We have presented evidence that the physical separation between paired sensory apertures predicts the depth of the neural processing hierarchy, across human sensory modalities, across mammalian and insect species, and across seven edge-case taxa spanning vertebrates and arthropods. The crepuscular prediction extends the framework from neuroanatomy to sensory morphology: animals that live at the beauty function peak have built their photoreceptor hardware at the edge of criticality.

The individual anatomical facts are well known. What we claim is novel is the unifying principle. The anatomy of the face is a map of the processing hierarchy. The geometry of the body is the temporal grammar written in tissue. The same three equations and one parameter that govern the cochlea also govern the eye, the nose, the fingertip, and — perhaps — the day and the night.

Companion Simulations

The Ω of Earth — day-night as CRR

WebGL simulation: SO(2) rotation, Z_2 terminator, beauty zones at dawn and dusk, city lights as rupture events. https://www.cohere.org.uk/crr_earth.html

The Divine Eye — vision on S^2

WebGL raytraced human eye: corneal Z_2 inversion, iris SO(2) collagen fibres, pupil as Dirac delta aperture. https://www.cohere.org.uk/divine_eye(CRR).html

The Living Cochlea — hearing on S^1

Basilar membrane with live microphone FFT, tonotopic CRR agents. https://www.cohere.org.uk/cochlea_crr_live.html

The Living Fingertip — touch as heatmap

RA onset/offset (Z_2) and SA sustained pressure (SO(2)) as thermal precision maps. https://www.cohere.org.uk/fingertip_heatmap_crr.html

The Living Nose — olfaction

Olfactory system: nasal cavity, epithelium, olfactory bulb, theta/gamma phase-gating. https://www.cohere.org.uk/nose_crr.html

References

Baker, G.T. and Ma, P.W.K. (2006). Morphology and number of ommatidia in the compound eyes of Solenopsis invicta. Zoologischer Anzeiger, 245, 121-125.

Beggs, J.M. & Plenz, D. (2003). Neuronal avalanches in neocortical circuits. J. Neurosci., 23, 11167–11177.

Bergson, H. (1896). Matter and Memory. London: George Allen and Unwin.

Čencov, N.N. (1982). Statistical Decision Rules and Optimal Inference. AMS.

Cocchi, L. et al. (2017). Criticality in the brain. Prog. Neurobiol., 158, 132–152.

Dodgson, N. (2004). Variation and extrema of human interpupillary distance. Proc. SPIE, 5291, 36-46.

Eastman, C.I. et al. (2015). Circadian rhythm phase shifts. Sci. Rep., 5, 8381.

Ezaki, T. et al. (2020). Closer to critical resting-state neural dynamics in individuals with higher fluid intelligence. Commun. Biol., 3, 52.

Felleman, D.J. and Van Essen, D.C. (1991). Distributed hierarchical processing in the primate cerebral cortex. Cereb. Cortex, 1, 1-47.

Grothe, B. (2003). New roles for synaptic inhibition in sound localization. Nat. Rev. Neurosci., 4, 540-550.

Hobson, J.A. and Friston, K.J. (2012). Waking and dreaming consciousness. Prog. Neurobiol., 98, 82-98.

Hoel, E. (2021). The overfitted brain. Patterns, 2(5), 100244.

James, W. (1890). The Principles of Psychology. New York: Henry Holt.

Jaynes, E.T. (1957). Information theory and statistical mechanics. Phys. Rev., 106, 620-630.

Jeon, C.J. et al. (1998). The major cell populations of the mouse retina. J. Neurosci., 18, 8936–8946.

Kinouchi, O. & Copelli, M. (2006). Optimal dynamical range of excitable networks at criticality. Nat. Phys., 2, 348–351.

Kopp-Scheinpflug, C. et al. (2016). Neurons in the medial superior olive of the mouse. J. Neurophysiol., 116, 2676-2688.

Kryger, Z. et al. (1998). Photoreceptor types in the California ground squirrel. Vis. Neurosci., 15, 851–866.

Müller, B. & Peichl, L. (1989). Topography of cones and rods in the tree shrew retina. J. Comp. Neurol., 282, 610–620.

Narendra, A. et al. (2011). Caste-specific visual adaptations in Myrmecia ants. Proc. R. Soc. B, 278, 1141-1149.

Parr, T., Pezzulo, G. and Friston, K.J. (2022). Active Inference. MIT Press.

Peichl, L. (2005). Diversity of mammalian photoreceptor properties. Anat. Rec. A, 287, 1001–1012.

Sabine, A. (2026a). Without Contraries There Is No Progression. Active Inference Institute.

Sabine, A. (2026b). Phase-gating across precision channels. Proc. AGI 2026 Workshop.

Saldana, E. et al. (2024). Medial superior olive in the rat. Hear. Res., 449, 109036.

Schwarz, S. et al. (2011). The visual system in Melophorus bagoti. Arthropod Struct. Dev., 40, 128-134.

Shew, W.L. & Plenz, D. (2013). Functional benefits of criticality in the cortex. Neuroscientist, 19, 88–100.

Strauss, M. et al. (2015). Disruption of hierarchical predictive coding during sleep. PNAS, 112, E1353-E1362.

Szél, Á. & Röhlich, P. (1992). Two cone types of rat retina. Neuroscience, 47, 961–971.
van der Merwe, I. et al. (2018). Rods, cones and ipRGCs in nocturnal and diurnal rodents. PLoS ONE, 13, e0202115.
Whitehead, A.N. (1929). Process and Reality. New York: Macmillan.
Zube, C. et al. (2008). Olfactory pathway in Camponotus floridanus. J. Comp. Neurol., 506, 425-441.

CRR computational method pending peer review. Active Inference Institute, 2026. Contact: Alexander@activeinference.institute